A Journal of the Gesellschaft Deutscher Chemiker

Angewandte International Edition Chemie

GDCh

www.angewandte.org

Accepted Article

Title: Direct imaging of atomically dispersed Mo enables locating Al in the framework of zeolite ZSM-5

Authors: Lingmei Liu, Ning Wang, Chongzhi Zhu, Xiaona Liu, Yihan Zhu, Peng Guo, Lujain Alfilfil, Xinglong Dong, Daliang Zhang, and Yu Han

To be cited as: *Angew. Chem. Int. Ed.* 10.1002/anie.201909834
Angew. Chem. 10.1002/ange.201909834

Link to VoR: http://dx.doi.org/10.1002/anie.201909834
http://dx.doi.org/10.1002/ange.201909834

WILEY-VCH

Direct imaging of atomically dispersed Mo enables locating Al in the framework of zeolite ZSM-5

Lingmei Liu,[a] Ning Wang, [a] Chongzhi Zhu,[b] Xiaona Liu,[c][d] Yihan Zhu,[b] Peng Guo,[c] Lujain Alfilfil,[a] Xinglong Dong,[a] Daliang Zhang,[e] Yu Han[a],*

[a] King Abdullah University of Science and Technology (KAUST), Physical Sciences and Engineering Division, Advanced Membranes and Porous Materials (AMPM) Center, Thuwal 23955-6900, Saudi Arabia

[b] Department of Chemical Engineering, Zhejiang University of Technology, Hangzhou 310014, P.R. China

[c] National Engineering Laboratory for Methanol to Olefins, Dalian National Laboratory for Clean Energy, Dalian Institute of Chemical Physics, Chinese Academy of Sciences, Dalian 116023, China

[d] University of Chinese Academy of Sciences, Beijing 100049, China

[e] Multi-scale Porous Materials Center, Institute of Advanced Interdisciplinary Studies & College of Materials Science and Engineering, Chongqing University, Chongqing 400044, P. R. China

* Correspondence to: yu.han@kaust.edu.sa

Abstract

Zeolites often act as host materials to encapsulate guest molecules to enrich their functions and applications, particularly in heterogeneous catalysis. Unfortunately, directly imaging guest molecules residing in the intact microporous structure of a zeolite has long been a challenge. Here, we report that integrated differential phase-contrast scanning transmission electron microscopy (iDPC-STEM) is capable of directly probing guest molecules in zeolites, due to its sufficient and interpretable image contrast for both heavy and light elements under low-dose conditions. We first demonstrate this unique ability by imaging volatile organic compounds adsorbed in zeolite Silicalite-1; we then use iDPC-STEM to investigate molybdenum supported on various zeolites including Silicalite-1, ZSM-5, and mordenite. We observe isolated single-Mo clusters in the micropores of ZSM-5, and demonstrate the crucial role of framework Al in driving Mo atomically dispersed into the micropores. Importantly, the specific one-to-one Mo-Al interaction makes it possible to locate Al atoms, i.e. catalytic active sites, in the ZSM-5 framework from the images, according to the positions of Mo atoms in the micropores. Our results indicate the feasibility of directly imaging guest components in fragile crystals at atomic resolution, paving the way to investigate host-guest interactions in nanoporous materials in unprecedented detail.

Introduction

Zeolites contain ordered intra-crystalline micropores that are often used to encapsulate various guest components (ions, molecules, and clusters) for specific catalytic applications.[1] The well-defined microporous structure is ideal for investigating the interaction between the confined guest component and the zeolite framework, allowing a better understanding of the synergetic relationship between the host and guest components.[2] However, although aberration-corrected electron microscopy has the ability to resolve single atoms, imaging guest components encapsulated in zeolites remains a considerable challenge, mainly because the crystalline structure of zeolite can be easily damaged by the electron beam. High-resolution transmission electron microscopy (HRTEM) performed with ultra-low doses of electron largely avoids the structural damage issue, but it is tricky to recognize or locate guest components with this technique because the image contrast obtained with HRTEM is difficult to interpret, as a result of the complicated effect imposed by the contrast transfer function of the objective lens.[3] Another commonly used imaging technique, high-angle annular dark-field scanning transmission electron microscopy (HAADF-STEM), is also a poor choice, despite its easily interpretable image contrast, due to the fact that it only uses a very small fraction of the incident electrons (those scattered to high angles), producing insufficient signals under the low-electron-dose conditions required to preserve the fragile structure of zeolites.[4] Consequently, guest components in zeolites are mostly invisible by HAADF-STEM, unless they are composed of heavy elements with a high loading.[2a, 5]

Molybdenum (Mo)- supported on aluminosilicate zeolite ZSM-5 (Mo-ZSM-5) is an effective bifunctional catalyst for the methane dehydroaromatization (MDA) reaction that allows a direct conversion of methane into aromatics and hydrogen without the participation of oxygen.[6] The catalytic roles of Mo and ZSM-5 in MDA have been extensively studied, and the most widely accepted reaction mechanism is the following: during the reaction, the C-H bonds in CH_4 are activated on the Mo sites to yield C_2H_x species that are further oligomerized and cyclized on the acid sites of ZSM-5 to form aromatics.[7] As a standard procedure of preparing the Mo-ZSM-5 catalyst, the mixture of $(NH_4)_6Mo_7O_{24}{\cdot}4H_2O$ (Mo precursor) and ZSM-5 is heated at 700 ^oC for several hours to yield Mo (IV) oxide species dispersed in the micropores of ZSM-5. Previous

studies suggest that there is one-to-one correspondence between the single-Mo oxide cluster ($Mo(=O)_2(OH)^+$) and the $[AlO_4]^-$ site in the zeolite framework, when the Si/Al and Al/Mo ratios are proper. [8] However, these studies are all based on the spectroscopic analysis of X-ray absorption, Raman, and ultraviolet-visible diffuse reflectance, [9] and a more direct evidence of the presence of Mo single atoms in the micropores of ZSM-5, for example by real-space imaging, has been so far unavailable. On the other hand, if the specific Mo-Al charge interaction, presumably leading to Mo off center of the micropore, can be visualized by direct imaging, it would be possible to locate Al atoms in the ZSM-5 framework, according to the positions of the Mo atoms. This has important implications for understanding zeolite-catalyzed reactions, given that Al atoms in zeolite framework correspond to catalytic active, Brönsted acid sites, where the reactions take place. Nuclear magnetic resonance spectroscopy, X-ray diffraction refinement, and atom probe tomography have been used to probe the distribution of Al among the crystallographically distinct T-sites in zeolites. [10] However, identifying Al from the surrounding Si atoms in a zeolite framework by direct electron microscopy imaging has not been achieved in the literature.

In this study, we demonstrate that integrated differential phase-contrast STEM (iDPC-STEM), [11] which makes full use of electron beam and has easily interpretable image contrast, is a powerful tool for imaging guest components in zeolites. Using iDPC-STEM, we successfully observe volatile organic compound (VOC) molecules adsorbed in zeolite Silicalite-1, and atomically dispersed, off-center Mo in 10-member-ring micropores in the Mo-ZSM-5 catalyst. In combination with theoretical modeling, the iDPC-STEM images allow us to locate Al atoms in the framework of ZSM-5 with a high Si/Al ratio.

Results and Discussion

As an emerging atomic-resolution imaging technique, iDPC-STEM makes use of almost all the electrons that interact with the specimen to form phase-contrast images, using a segmented detector (Supporting Information, Figure S1). [11a, 12] It has been established that iDPC-STEM shows the best contrast and signal-to-noise ratio (SNR), in comparison with standard bright-field and dark-field STEM modes for the same probe conditions. [11a, 13] The contrast of iDPC image can

be easily interpreted, as it approximately corresponds to the local electrostatic potential field of the thin specimen being probed. Moreover, iDPC-STEM allows the simultaneous imaging of heavy and light elements. [11b]

The advantages of iDPC-STEM outlined above make this technique, in principle, an excellent choice for probing guest components encapsulated in microporous structures of zeolites. To verify this hypothesis, we first perform low-dose STEM (beam current: 1 pA; total dose: 1128 $e^-/Å^2$) to observe freshly calcined Silicalite-1, a pure-silica zeolite with a MFI-type framework, along its [010] zone axis, and acquire HAADF and iDPC images simultaneously for comparison purposes (Figures 1a-1b). Note that the employed low-dose condition is necessary to preserve the structural integrity of zeolites during the observation. The ǋI·ǘKŜǋ ΨyƻƛǎềΩ HAADF-STEM image (Figure 1a) only shows clearly the primary 10-member-ring (MR) straight channels of MFI; however, the structural details of the framework (e.g., 6-MR and 5-MR secondary building units) are blurred, due to the poor SNR associated with the low electron dose. By comparison, the iDPC image formed by the same electron probe (Figure 1b) shows remarkably stronger signals and thus sharper contrast, allowing each individual Si atom in the framework to be clearly resolved. The better resolution of the iDPC image, compared to the HAADF image (1.2 Å *vs*. 1.6 Å), is confirmed by Fourier transforms (FTs) of the images (Supporting Information, Figure S2). This result demonstrates the importance of SNR to the resolving power of the image under low-dose conditions.

After exposing the Silicalite-1 sample to air for two weeks, we observe it again with STEM, using identical imaging conditions. Very interestingly, we note that the iDPC-STEM image (Figure 1d) shows a strong contrast in the 10-MR channels. This is strikingly different from the freshly calcined sample that shows clear and clean channels, without any contrast inside (Figure 1b). The contrast observed in air-exposed silicalite-1 varies in shape and orientation in different channels (Figure 1d), ruling out the possibility of imaging artifact. More interestingly, this contrast disappears from the iDPC-STEM image (the channels ǋŜǘdzǋƴ ǘƻ ōŜ άŜƳǊǘềέ) when we re-calcine the sample in air at 823 K before STEM imaging (see Figure 1f), suggesting that the contrast is related to organic compounds that can be removed by calcination. HAADF-STEM images of air-exposed and re-calcined Silicalite-1 samples are presented in Figures 1c and 1e, respectively.

Figure 1c shows no sign of guest molecules existing in the 10-MR channels. Taken together, these observations indicate that Silicalite-1 adsorbs molecules of volatile organic compound (VOC) into the 10-MR channels when exposed to the air, and that these guest molecules can be directly imaged by iDPC-STEM but not by HAADF-STEM. Note that the observed image contrast represents an averaged electrostatic potential within the ά depth of field έ of the electron beam probe along the projection direction. The imaging conditions used in this study render I· άŘŜŁJűK 2Ŧ ŦλŜfŘέ of ~ 16 nm, as calculated from the convergence angle and the wavelength of the electron beam.[14] Therefore, we do not claim single-molecule-level sensitivity for our images. We alternatively probed the absence or presence of guest species in large MFI zeolite crystals by powder X-ray diffraction (PXRD); the derived difference electron density maps show that the air-exposed sample has extra electron density in the 10-MR channels, in comparison with the freshly calcined sample (SI, Figure S3). This result is in good agreement with our iDPC-STEM observation, confirming the adsorption of VOC by MFI zeolite. The attempt to identify the exact adsorbed VOC species with combined thermogravimetry and mass spectrometry is unsuccessful due to their low contents (SI, Figure S4).

The aforementioned experiments demonstrate the unique ability of iDPC-STEM to visualize guest molecules in the micropores, under low-dose conditions, inspiring us to use it to investigate Mo species in a fresh Mo-ZSM-5 catalyst. To do so, we first synthesize a Mo-ZSM-5 catalyst with Si/Al^{o} 40 and Al/Mo^{o} 1 (see Experimental section for synthetic details and Table S1 for specific compositions), which is supposed to have single-Mo oxide clusters ($Mo(=O)_2(OH)^+$) dispersed in the micropores and bonded to single-Al sites ($[AlO_4]^-$) in the framework, according to the systematic spectroscopic study by Gao *et al*. [9b] For comparison purposes, we prepare another sample, Mo-Silicalite-1, following the same procedure except that the support material is pure-silica (Al-free) zeolite Silicalite-1. All the peaks in the powder X-ray diffraction (PXRD) pattern of Mo-ZSM-5 can be indexed to the MFI structure, revealing the absence of a bulk crystalline phase of Mo in this sample; in contrast, the PXRD pattern of Mo-Silicalite-1 shows additional peaks at 2q = 12.7 and 27.3^{o} that correspond to the (020) and (021) reflections of the MoO_3 phase, respectively (Figure 2a). The PXRD results indicate that despite the same loading amount (~2.5 wt%), Mo oxide species is highly dispersed (or in the form of small clusters) in Mo-ZSM-5, but

forms bulk MoO_3 crystals in Mo-Silicalite-1. The different forms of Mo in the two samples are also evidenced by Raman spectroscopy. As shown in Figure 2, Mo-Silicalite-1 has two intense Raman bands at 995 cm^{-1} and 818 cm^{-1} that are characteristic of the bulk crystalline MoO_3 phase, [9b, 15] whereas Mo-ZSM-5 gives several broad bands, among which the ones at ϕcϕ»0Y^{-1} and 982 cm^{-1} have been assigned to the Mo=O stretching mode of atomically dispersed MoO_X clusters confined in ZSM-5 channels and bound to surface Si sites, respectively, in the literature. [9b] Our Mo-ZSM-5 sample shows a very weak Raman band at 992 cm^{-1}, which is assigned to the Mo-O stretching mode of single-Mo cluster anchored on double-Al (Al pair) sites. [9b] This result suggests the lack of adjacent Al atoms in the ZSM-5 sample, which is consistent with its relatively high Si/Al ratio.

Energy dispersive spectroscopy (EDS) elemental mapping performed under STEM shows that Mo species are concentrated and form large particles (tens of nanometer in size) on Silicate-1 (Figure 2c), but are highly dispersed on ZSM-5 (Figure 2d), confirming the conclusion drawn from PXRD and Raman spectroscopy. The higher degree of Mo dispersion on ZSM-5 must be related to its Al species, as this is the only difference between the two support materials. Elemental mapping also reveals that Al is not uniformly distributed over the entire ZSM-5 crystal, but more enriched at the crystal periphery, in agreement with other previous studies. [16] Interestingly, the distribution of Mo is found to coincide with that of Al, indicating a close correlation between Mo and Al (Figure 2d), and thus the crucial role that the framework Al plays in promoting the Mo species to atomically disperse into zeolite crystals.

Figure 3a shows an atomic-resolution iDPC-STEM image of freshly prepared Mo-ZSM-5, in which a weak, yet clearly identifiable, contrast is observed in most 10-MR channels. In comparison with the case of air-exposed Silicalite-1 (Figure 1d), the contrast observed here is weaker in intensity but more focused, suggesting a different guest species from VOCs. In fact, freshly prepared Mo-ZSM-5 (loading Mo on ZSM-5 by heating at 700 °C in air) should not contain VOCs, according to our aforementioned study (Figures 1b and 1f). Moreover, unlike the case of air-exposed Silicalite-1 where the extra contrast appears at the center of channels (Figure 1d), the contrast observed in Mo-ZSM-5 is apparently off center of the channels (Figure 3a). In addition, the iDPC-STEM image of the Mo-Silicalite-1 acquired under exactly the same conditions shows clean 10-MR channels (Figure 4a). On the basis of these observations and considerations,

we assign this extra contrast in the channels of ZSM-5 to atomically dispersed Mo oxide species ($Mo(=O)_2(OH)^+$) I·yŘ I·úúNλōdzűŜ úKŜ á2₸₸ ŎŜyűŜNɛ ŎKI·NI·ŎűŜNλăűλŎ ű2 λűă ōλnding to a single $[AlO_4]^-$ site in the surrounding framework. This is the first time that a single-atom Mo species has been directly observed and that its interaction with the zeolite framework been visualized.

The ZSM-5 sample has a Si/Al of 40, corresponding to one Al atom in one projected 10-MR channel per unit cell in average. The low Al content combined with the fact that atomic-resolution image is acquired from ultra-thin area of the specimen increases the probability of seeing only one Mo cluster in each projected 10-MR channel (Figure 3a). Under such a situation, the one-to-one Mo-Al correspondence allows the identification of the single Al site out of 10 T atoms that comprise the channel, according to the position of Mo. Figures 3b-3d show enlarged images of three representative channels: empty channel (Fig. 3b), and channels containing a Mo cluster bound at the T_8 site (Fig. 3c) and T_1 site (Fig. 3d). The intensity profiles analysis (Fig. 3e) indicates a marked separation (0.79 Å) in the Mo position between the two channels shown in Figs. 3c and 3d, illustrating that the single-Mo oxide clusters anchor on different T-sites. Therefore, we use Mo as a probe to locate Al around the 10-MR channel, and make a simple statistic based on the observations of one hundred channels. Results show that Al most preferentially occupies the T_1 site (40%), followed by the T_2 and T_5 sites, and disfavors the T_3 and T_6 sites (Fig. 3f). Because the two opposing T sites around the 10-MR ring (e.g., T_1 *vs*. T_7, T_2 *vs*. T_8) are overlapping to each other along the projected [010] direction, they are combined in the statistical analysis. The T sites preferred by Al in the framework of ZSM-5 have been investigated in the literature, mainly by single-crystal or powder X-ray diffraction refinement.[10c, 17] Several independent works based on Cs-exchanged ZSM-5 consistently conclude that Al most preferentially occupies the T_7 site.[17] This conclusion is in agreement with our observation that unfortunately cannot distinguish T_7 and T_1 sites.

The DFT calculations indicate that the Mo species selectively anchor on the Al sites when placed in the 10-MR channels of ZSM-5. For a given T site, the calculated binding energy (BE) of a single-Mo cluster ($Mo(=O)_2(OH)^+$) at AlO_4 is always higher than that at SiO_4 (for instance, $BE_{(Al)}$ *vs*. $BE_{(Si)}$ = -2.90 eV *vs*. -1.35 eV, at the T_1 site; $BE_{(Al)}$ *vs*. $BE_{(Si)}$ = -2.61 eV *vs*. -1.59 eV, at the T_8 site). The DFT-optimized structural models of empty channel, and channels with the single-Mo cluster

anchored at the T_8 and T_1 sites are used to simulate the projected electrostatic potential maps, which show a good match with the corresponding experimental iDPC-STEM images (Fig. 3b). These results validate the hypothesis that Mo can act as a marker to locate Al in the framework of ZSM-5.

We have also successfully imaged Mo species dispersed in the microporous channels of other types of zeolites, using iDPC-STEM. When zeolite mordenite that has larger pores and a higher Al content (Si/Al^{o} 6) than ZSM-5 is used as the support (SI, Table S1), Mo is also highly dispersed throughout the zeolite crystal without the formation of bulk MoO_3 phase, as determined by EDS elemental mapping and PXRD characterizations (SI, Figure S5). In the high-resolution iDPC-STEM image, an extra weak contrast is also observed in the 12-MR straight channels (Figure 4b). Interestingly, the observed contrast is more diffuse and elongated, compared to that obtained with Mo-ZSM-5. This may be because of the increased pore size and Al content, which favors the formation of bigger Mo clusters (e.g., $Mo_2O_5^{2+}$) interacting with Al pairs or leads to the presence of multiple single-Mo clusters residing in the channels along the projection direction.

It is worth noting that in principle, the Al sites can also be identified by imaging commonly used basic probe molecules, such as ammonia (NH_3) and pyridine, because the basic molecules specifically bind to the Al sites through acid-base interactions. However, our attempts of imaging NH_3- or pyridine-adsorbed ZSM-5 reveal that NH_3 is difficult to identify even using iDPC-STEM, while chemically adsorbed pyridine molecules can be observed, but their diffuse and blurred contrast leads to inconclusive assignments of Al sites (SI, Fig. S6).

Conclusions

In this paper, we report the successful imaging of guest components, including physically adsorbed VOC molecules and chemically bound single-Mo oxide clusters, in the micropores of various zeolites by iDPC-STEM. Our images provide the first direct evidence of the atomic dispersion of Mo species, in a Mo-ZSM-5 catalyst. Through control experiments, we demonstrate that it is the framework Al that promotes the Mo species to disperse into the 10-MR channels of ZSM-5 through specific Mo-Al interactions. This specific interaction drives Mo off the center of

the channel towards the single Al site, making it possible to distinguish Al atoms from Si atoms, in the framework, based on the positions of Mo determined from the atomic-resolution images. Given that the framework Al atoms correspond to Brönsted acid sites, our study provides a method to locate catalytic active centers in zeolite-catalyzed reactions. We also find that the dimensions of the micropore and the content of framework Al may impact on the form of the encapsulated Mo species. The use of iDPC-STEM opens new opportunities for directly studying host-guest interactions in real space; its high imaging performance, under low-dose conditions, is particularly valuable for investigating materials that are unstable under electron beams.

Experimental Section

Preparation of samples

Zeolites Silicalite-1, ZSM-5 (Si/Al^{o} 40) and Mordenite (Si/Al^{o} 6) were synthesized following previously reported procedures. [18] After the synthesis, the zeolite samples were all calcined at 550^{o}C for 6 h to remove organic structural directing agents.

The calcined Silicalite-1 was exposed to air, in ambient conditions, for two weeks, and the obtained sample referred to as ΨI·ЖЩ-exposed Silicalite-1Ω. The air-exposed Silicalite-1 was calcined in air at 550 ^{o}C for 6h again to remove the adsorbed VOCs, and the obtained sample referred to as ΨЩŜ-calcined Silicalite-1Ω.

The Mo-ZSM-5 catalyst was prepared by incipient wetness impregnation, using ammonium heptamolybdate tetrahydrate ($(NH_4)_6Mo_7O_{24}\cdot 4H_2O$) as the Mo precursor. Typically, 0.074 g of $(NH_4)_6Mo_7O_{24}\cdot 4H_2O$ was dissolved in 2 mL of distilled water; 1g of calcined ZSM-5 powder was added into the solution (Al/Mo=1; in molar). After stirring for 2h, the mixture was dried in an oven, overnight, at 110℃. The obtained powder was dried at 350 ^{o}C for 24 h, in flowing air, and then heated at 10 ^{o}C/min to 700 ^{o}C and hold at 700 ^{o}C for 2h. Mo-Silicalite-1 was prepared following the same procedure, except that ZSM-5 was replaced by the same amount of Silicalite-1 as the support material. Mo-Mordenite was also prepared using the same method, while the amount of $(NH_4)_6Mo_7O_{24}\cdot 4H_2O$ was adjusted to achieve Mo/Al=0.20 (in molar).

Electron microscopy imaging conditions

STEM experiments were performed using a double Cs-corrected microscope (FEI Titan Cubed Themis Z), operated at 300 kV. The microscope was aligned prior to each experiment, using a cross-grating standard sample. Specimen searching and zone axis alignment were carried out at a 13000× magnification, under the TEM mode. After alignment of the crystal zone axis, the microscope was switched to the STEM mode with a convergence semi-angle of 11.0 mrad to acquire iDPC- and HAADF-STEM images simultaneously. The probe current was ~1 pA, pixel size is 0.2576 Å, and the dwell time is 12 µs/pixel, corresponding to a total electron dose of 1128 $e^-/Å^2$. iDPC-STEM images were acquired using a 4-quadrant DF4 detector with a high-pass filter applied on to reduce the low frequency information, and HAADF-STEM images were acquired using a HAADF detector. The collection angle of iDPC was set as 5-21 mrad, and the collection angle of HAADF detector at this experimental condition was 22-135 mrad.

Calculations and simulations

Plane-wave based DFT calculations were carried out on a ZSM-5 unit cell with 96 T atoms and 192 oxygen atoms using the CASTEP code. For Mo-free (zeolite framework alone) geometries, a single Al site was embedded in the framework at T1 site with a charge-balancing proton at atop site of the neighboring bridge oxygen. For Mo-containing geometries, monovalent $[MoO_3H]^+$ species was included inside the 10-membered ring (MR) in the vicinity of either T1 or T8 site. The binding energy (BE) of $[MoO_3H]^+$ on a T site of the ZSM-5 framework was calculated as BE = ([MoO_3H]-ZSM-p ώah_3] + H-ZSM-5). Calculations were based on the PerdewçBurkeç Ernzerhof exchange-correlation functional using generalized gradient approximation. Only the gamma-point of the first Brillouin zone was sampled due to the large zeolite cells. The geometries were relaxed upon the convergence tolerances for electronic energy and maximum force of 5 ³ 10^{-5} eV/atom and 0.1 eV/Å, respectively. The projected electrostatic potential were simulated by the QSTEM software [19], with point spread function width of 1.8Å.

Acknowledgements

This research was supported by CCF grant (FCC/1/1972-19) to Y.H. from King Abdullah University 2Ŧ {ŎʎŜyŎŜ I·yŘ ¢ŜŎKy2f2Ǝè óY!¦{¢úφ ¢Kʎă ℕŜăŜI·ℕŎK dzăŜŘ űKŜ ℕŜă2dzℕŎŜă 2Ŧ Y!¦{¢Ωă /2ℕŜ [I·ōă

facilities. Y. Z. acknowledges financial support from National Natural Science Foundation of China (21771161) and the Thousand Talents Program for Distinguished Young Scholars. D. Z. acknowledges financial support from Fundamental Research Funds for the Central Universities (02200052020013).

References

[1] a) M. E. Davis, *Nature* 2002, *417*, 813-821; b) L. C. Liu, U. Díaz, R. Arenal, G. Agostini, P. Concepción, A. Corma, *Nat. Mater.* 2017, *16*, 132-138; c) Q. W. Tian, Z. H. Liu, Y. H. Zhu, X. L. Dong, Y. Saih, J. Basset, M. Sun, W. Xu, L. K. Zhu, D. L. Zhang, J. F. Huang, X. J. Meng, F. S. Xiao, Y. Han, *Adv. Funct. Mater.* 2016, *26*, 1881-1891.

[2] a) J. D. Kistler, N. Chotigkrai, P. H. Xu, B. Enderle, P. Praserthdam, C. Y. Chen, N. D. Browning, B. C. Gates, *Angew. Chem. Int. Ed.* 2014, *53*, 8904-8907; b) J. Zhang, L. Wang, B. S. Zhang, H. S. Zhao, U. Kolb, Y. H. Zhu, L. M. Liu, Y. Han, G. X. Wang, C. T. Wang, D. S. Su, B. C. Gates, F. S. Xiao, *Nat. Catal.* 2018, *1*, 540-546; c) L. C. Liu, R. Arenal, D. M. Meira, A. Corma, *Chem. Commun.* 2019, *55*, 1607-1610.

[3] a) Y. H. Zhu, J. Ciston, B. Zheng, X. H. Miao, C. Czarnik, Y. C. Pan, R. Sougrat, Z. P. Lai, C. E. Hsiung, K. X. Yao, I. Pinnau, M. Pan, Y. Han, *Nat. Mater.* 2017, *16*, 532-536; b) D. L. Zhang, Y. H. Zhu, L. M. Liu, X. R. Ying, C. E. Hsiung, R. Sougrat, K. Li, Y. Han, *Science* 2018, *359*, 675-679; c) D. Aulakh, L. M. Liu, J. R. Varghese, H. M. Xie, T. Islamoglu, K. Duell, C. W. Kung, C. E. Hsiung, Y. X. Zhang, R. J. Drout, O. K. Farha, K. R. Dunbar, Y. Han, M. Wriedt, *J. Am. Chem. Soc.* 2019, *141*, 2997-3005. d) L. M. Liu, Z. J. Chen, J. J. Wang, D. L. Zhang, Y. H. Zhu, S. L. Ling, K.W. Huang, Y. Belmabkhout, K. Adil, Y. X. Zhang, B. Slater, M. Eddaoudi, Y. Han, *Nat. Chem.* 2019, *11,* 622-628; e) X. H. Li, J. J. Wang, X. Liu, L. M. Liu, D. Cha, X. L. Zheng, A. A. Yousef, K. P. Song, Y. H. Zhu, D. L. Zhang, Y. Han, *J. Am. Chem. Soc.* 2019, *141,* 12021-12028.

[4] a) Z. Liu, N. Fujita, K. Miyasaka, L. Han, S. M. Stevens, M. Suga, S. Asahina, B. Slater, C. H. Xiao, Y. Sakamoto, M. Anderson, R. Ryoo, O. Terasaki, *Microscopy* 2013, *62*, 109-146; b) A. Mayoral, M. Sanchez-Sanchez, A. Alfayate, J. Perez-Pariente, I. Diaz, *ChemCatChem* 2015, *7*, 3719-3724; c) A. Mayoral, R. M. Hall, J. Roksana, J. E. Readman, *Angew. Chem.* 2016, *128*, 16361-16365.

[5] a) V. Ortalan, A. Uzun, B. C. Gates, N. D. Browning, *Nat. Nanotechnol.* 2010, *5*, 506-510; b) A. Mayoral, T. Carey, P. A. Anderson, A. Lubk, I. Diaz, *Angew. Chem. Int. Ed.* 2011, *50*, 11230-11233.

[6] a) L. S. Wang, L. X. Tao, M. S. Xie, G. F. Xu, J. S. Huang, Y. D. Xu, *Catal. Lett.* 1993, *21*, 35-41; b) Z. R. Ismagilov, E. V. Matus, L. T. Tsikoza, *Energy Environ. Sci.* 2008, *1*, 526-541; c) P. Schwach, X. L. Pan, X. H. Bao, *Chem. Rev.* 2017, *117*, 8497-8520.

[7] a) A. Kumar, K. P. Song, L. M. Liu, Y. Han, A. Bhan, *Angew. Chem. Int. Ed.* 2018, *57* , 15577-15582; b) I. Lezcano-González, R. Oord, M. Rovezzi, P. Glatzel, S. T. Botchway, B. M. Weckhuysen, A. M. Beale, *Angew. Chem. Int. Ed.* 2016, *55*, 5215-5219; c) I. Vollmer, B. V. D. Linden, S. Ould-Chikh, A. Aguilar-Tapia, I. Yarulina, E. Abou-Hamad, Y. G. Sneider, A. I. O. Suarez, J. L. Hazemann, F. Kapteijn, J. Gascon, *Chem. Sci.* 2018, *9*, 4801-4807; d) M. Agote-Arán, A. B. Kroner, H. U. Islam, W. A. [illegible] D. S. Wragg, I. Lezcano-González, A. M. Beale, *ChemCatChem* 2019, *11*, 473-480.

[8] a) W. P. Ding, S. Z. Li, G. D. Meitzner, E. Iglesia, *J. Phys. Chem. B* 2001, *105*, 506-513; b) N. Kosinov, F. J. A. G. Coumans, E. A. Uslamin, A. S. G. Wijpkema, B. Mezari, E. J. M. Hensen, *ACS Catal.* 2017, *7*, 520-529.

[9] a) W. Li, G. D. Meitzner, R. W. Borry, E. Iglesia, *J. Catal.* 2000, *191*, 373-383; b) J. Gao, Y. T. Zheng, J. M. Jehng, Y. D. Tang, I. E. Wachs, S. G. Podkolzin, *Science* 2015, *348*, 686-690.

[10] a) S. Sklenak, J. 5ŠŘŜőŜ꞉Ȥ C. B. Li, B. Wichterlová, V. Gábová, M. Sierka, J. Sauer, *Angew. Chem. Int. Ed.* 2007, *46*, 7286-7289; b) S. Sklenak, J. 5ŠŘŜőŜ꞉Ȥ C. B. Li, Wichterlová, V. Gábová, M. Sierka, J. Sauer, *Phys. Chem. Chem. Phys.* 2009, *11*, 1237-1247; c) B. T. W. Lo, L. Ye, J. Qu, J. L. Sun, J. L. Zheng, D. J. Kong, C. A. Murray, C. C. Tang, S. C. E. Tsang, *Angew. Chem.* 2016, *128*, 6085-6088; d) D. E. Perea, I. Arslan, J. Liu, Z. wƛăű l·ƴϨǾƛŏȤ L. Kovarik, B. W. Arey, J. A. Lercher, S. R. Bare, B. M. Weckhuysen, *Nat. Commun.* 2015, *6*, 7589; e) Z. H. Liu, X. L. Dong, Y. H. Zhu, A.H. Emwas, D. L. Zhang, Q. W. Tian, Y. Han, *ACS Catal.* 2015, *5*, 5837-5845.

[11] a) I. [l·Îƛŏȥ E. G. T. Bosch, S. Lazar, *Ultramicroscopy* 2016, *160*, 265-280; b) E. Yücelen, I. [l·Îƛŏȥ E. G. T. Bosch, *Sci. Rep.* 2018, *8*, 2676.

[12] a) H. Yang, T. J. Pennycook, P. D. Nellist, *Ultramicroscopy* 2015, *151*, 232-239; b) T. J. Pennycook, A. R. Lupini, H. Yang, M. F. Murfitt, L. Jones, P. D. Nellist, *Ultramicroscopy* 2015, *151*, 160-167.

[13] H. Rose, *Ultramicroscopy* 1976, *2*, 251-267.

[14] A. Y. Borisevich, A. R. Lupini, S. J. Pennycook, *PNAS* 2006, 103, 3044-3048.

[15] E. L. Lee, I. E. Wachs, *J. Phys. Chem. C* 2007, *111*, 14410-14425.

[16] a) R. V. Ballmoos, W. M. Meier, *Nature* 1981, *289*, 782-783; b) J. C. Groen, T. Bach, U. Ziese, A. M. P. Donk, K. P. D. Jong, J. A. Moulijn, J. Pérez-Ramírez, *J. Am. Chem. Soc.* 2005, *127*, 10792-10793.

[17] a) C. W. Kim, N. H. Heo, K. Seff, J. Phys. Chem. C 2011, 115, 24823-24838; b) D. H. Olson, N. Khosrovani, A. W. Peters, B. H. Toby, J. Phys. Chem. B 2000, 104, 4844-4848; c) B. F. Mentzen, G. U. Bergeret, G. Bergeret, H. P. Weber, J. Phys. Chem. C 2006, 110, 97-106;

[18] a) Y. H. Ma, D. L. Cai, Y. R. Li, N. Wang, U. Muhammad, A. Carlsson, D. Tang, W. Z. Qian, Y. Wang, D. S. Su, F. Wei, RSC Adv. 2016, *6,* 74797-74801; b) Y. M. Mao, Y. Zhou, H. M. Wen, J. Y. Xie, W. Zhang, J. Wang, New J. Chem. 2014, *38,* 3295-3301.

[19] QSTEM V2, 31; www.qstem.org.

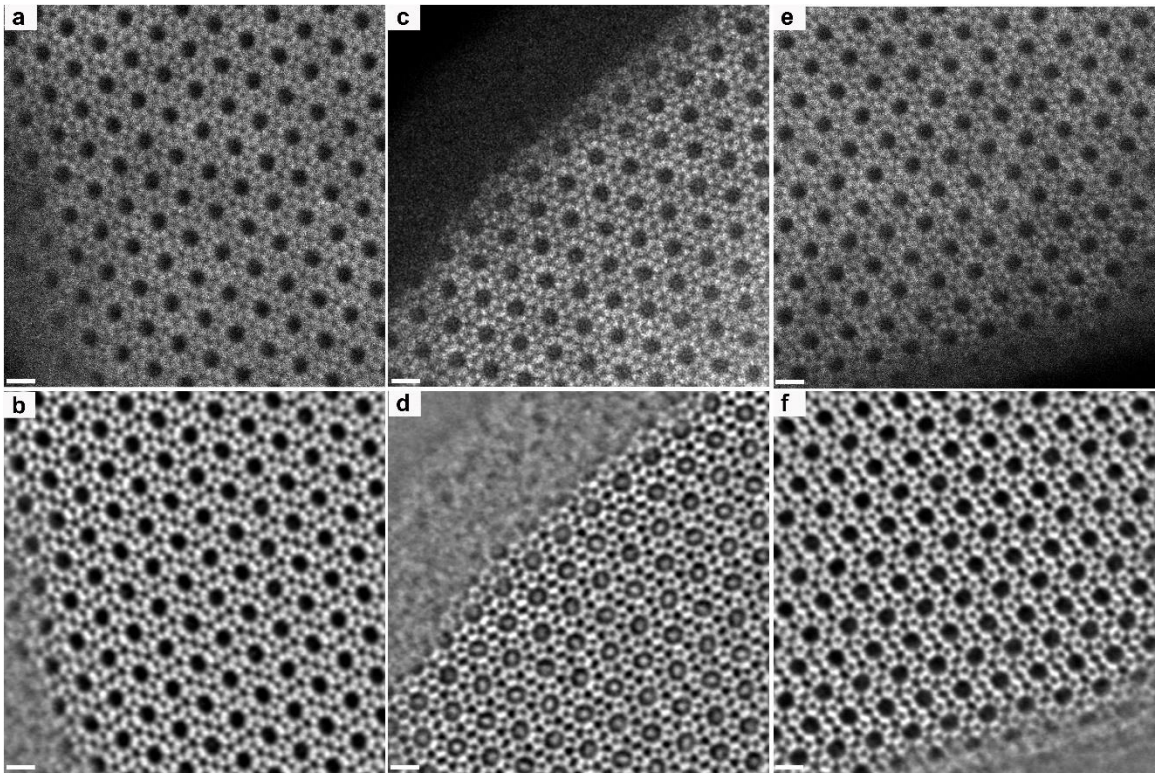

Figure 1. Simultaneously acquired HAADF-STEM (top) and iDPC-STEM (bottom) images of different silicalite-1 samples: (a, b) freshly prepared (calcined); (c, d) air-exposed; (e, f) re-calcined silicalite-1. The scale bars represent 1 nm.

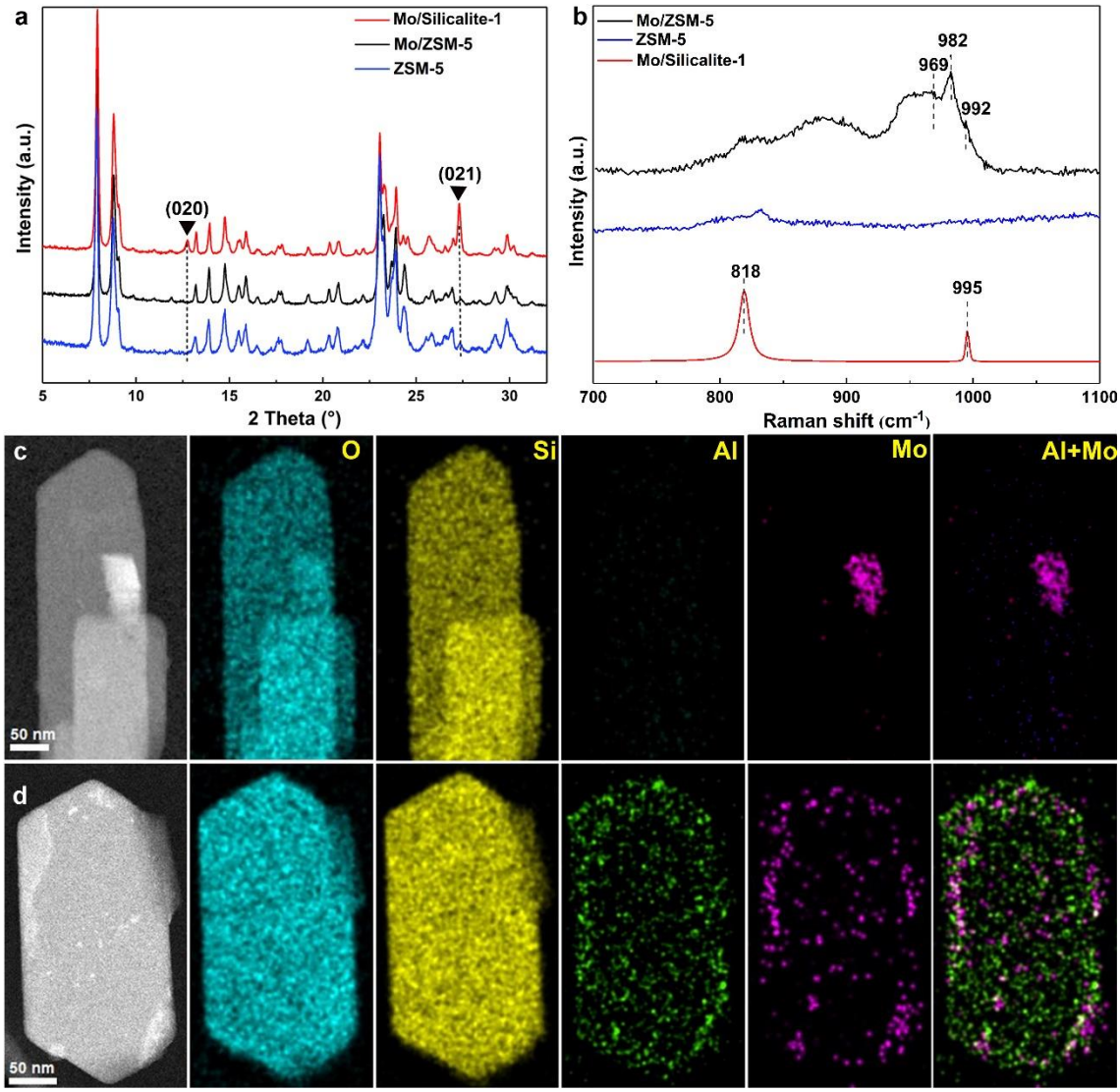

Figure 2. (a) PXRD patterns of ZSM-5, Mo/ZSM-5 and Mo/Silicate-1. Dotted lines indicated diffraction peaks associated with MoO_3 phase, which only appear in the pattern of Mo/Silicalite-1. (b) Raman spectra of ZSM-5, Mo/ZSM-5 and Mo/Silicate-1. (c-d) HAADF-STEM image (the left panel) and the corresponding EDS elemental maps (the rest panels, in which the element type is labelled at the upper right corners) of Mo/Silicate-1 (c) and Mo/ZSM-5 (d).

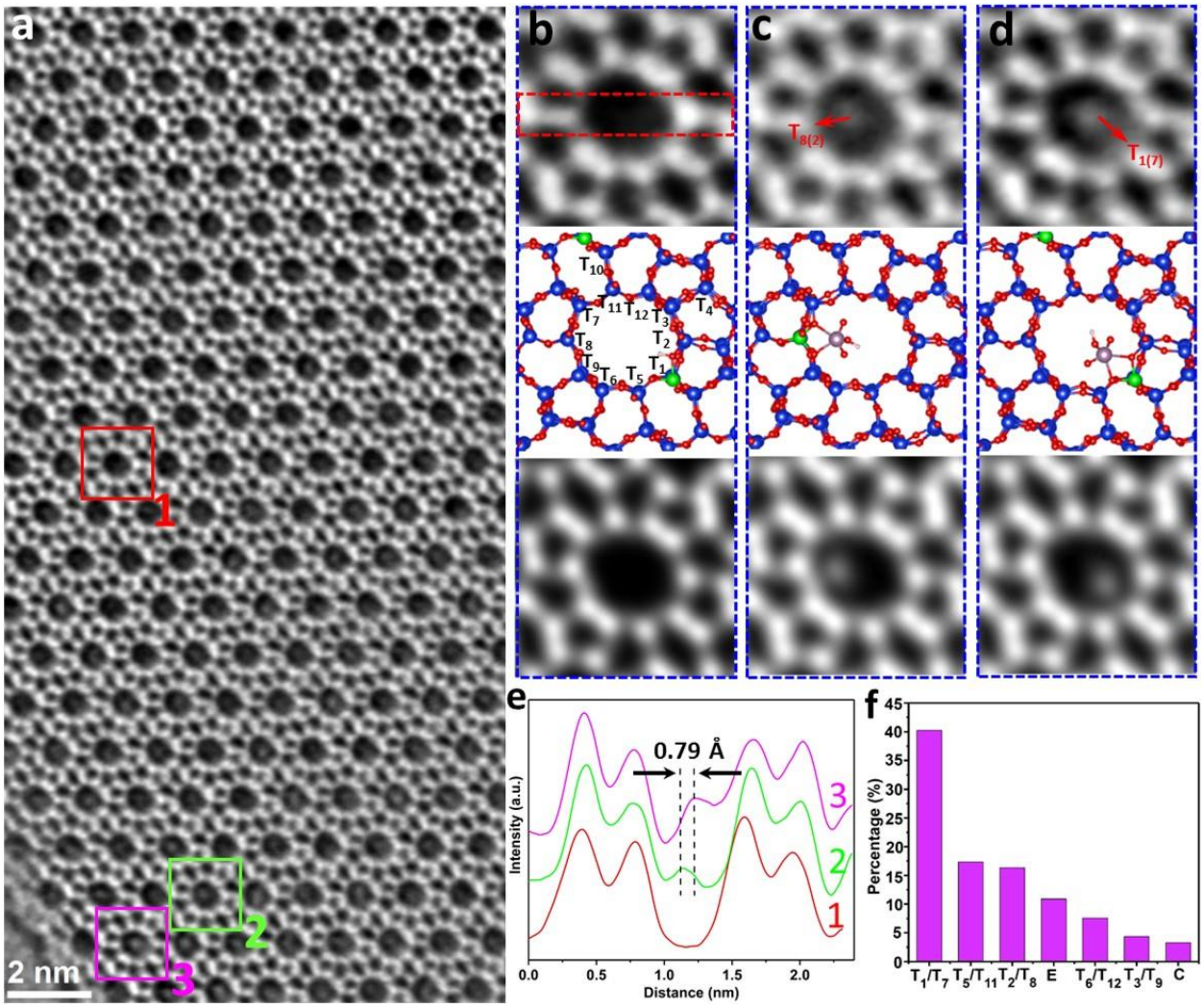

Figure 3. (a) A representative iDPC-STEM image of Mo/ZSM-5, showing the presence of off-center contrast in many 10-MR channels. (b, c, d) Zoomed-in areas 1, 2, and 3 of (a), respectively, corresponding to three scenarios: empty channel (b), and channels containing a MoO_3H cluster bound at the T_8 site (c) and at the T_1 site (d). Each panel includes the raw image (top), the calculated structural model (middle), and the simulated projected electrostatic potential (bottom). Atom color code in structural models: Si, blue; O, red; Al, green, Mo, pink; H, white. (e) Intensity line profiles of the images in (b), (c), and (d), across the areas as represented by the red dashed rectangle. (f) Statistics of Al occupancy at different T sites, based on the results of one hundred channels. ¢KŜ fI·ōŜfă á9é I·yŘ á/é ℕŜLJℕŜăŜyú ŜY˙LJúè ŎKI·yɣŜfă I·yŘ ŎKI·yɣŜfă with an on-center extra contrast, respectively.

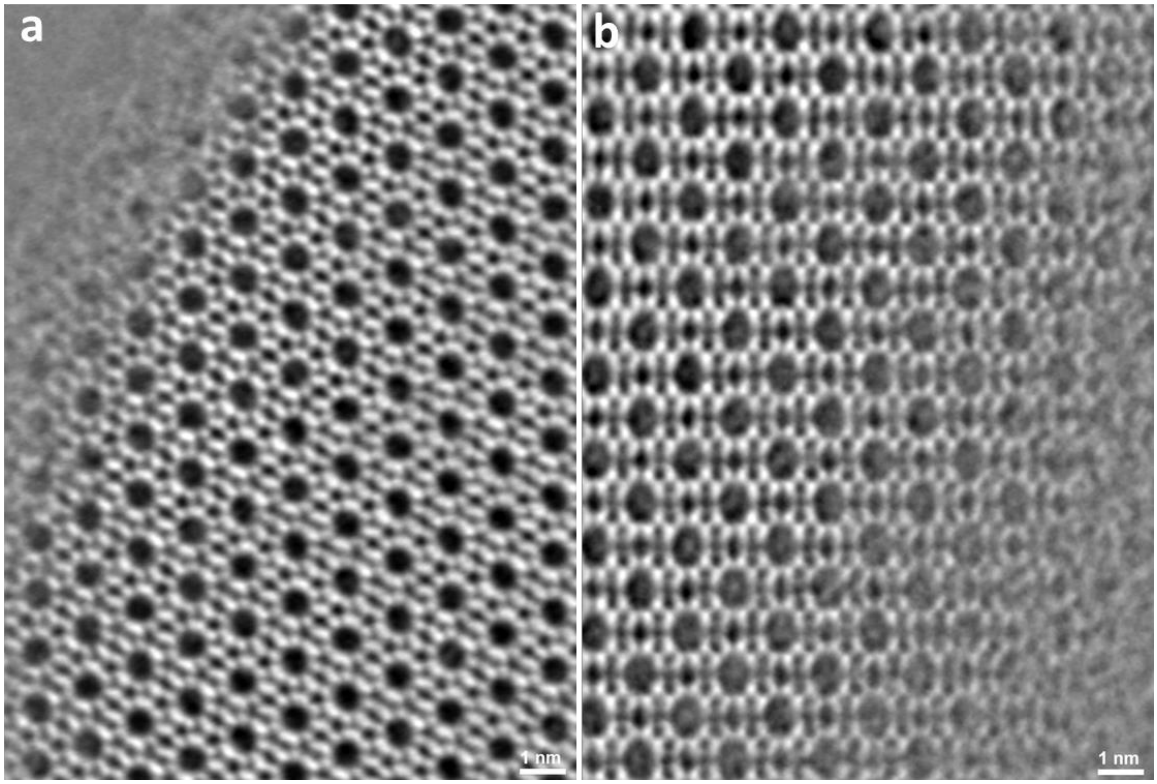

Figure 4. iDPC-STEM images of Mo/silicate-1 (a), and Mo/mordenite (b). No extra contrast is observed in the 10-MR channels in (a), indicating the absence of atomically dispersed Mo species in Silicalite-1; diffuse and elongated weak contrast is observed in some 12-MR channels in (b), suggesting the presence of Mo species in mordenite that are different from those in ZSM-5.